Check for updates

Mechanism of magnetisation relaxation in {M₂ᴵᴵᴵDy₂ᴵᴵᴵ} (M = Cr, Mn, Fe, Al) "Butterfly" complexes: how important are the transition metal ions here?†

Yan Peng, [ab] Mukesh Kumar Singh, [c] Valeriu Mereacre, [a] Christopher E. Anson, [a] Gopalan Rajaraman [*c] and Annie K. Powell [*ab]

We describe the synthesis, characterisation and magnetic studies of four tetranuclear, isostructural "butterfly" heterometallic complexes: [M₂ᴵᴵᴵLn₂ᴵᴵᴵ(μ₃-OH)₂(*p*-Me-PhCO₂)₆(L)₂] (H₂L = 2,2′-((pyridin-2-ylmethyl)azanediyl)bis(ethan-1-ol), M = Cr, Ln = Dy (**1**), Y (**2**), M = Mn, Ln = Dy (**3**), Y (**4**)), which extend our previous study on the analogous **5** {Fe₂Dy₂}, **6** {Fe₂Y₂} and **7** {Al₂Dy₂} compounds. We also present data on the yttrium diluted **7** {Al₂Dy₂}: **8** {Al₂Dy₀.₁₈Y₁.₈₂}. Compounds dc and ac magnetic susceptibility data reveal single-molecule magnet (SMM) behaviour for complex **3** {Mn₂Dy₂}, in the absence of an external magnetic field, with an anisotropy barrier U_{eff} of 19.2 K, while complex **1** {Cr₂Dy₂}, shows no ac signals even under applied dc field, indicating absence of SMM behaviour. The diluted sample **8** {Al₂Dy₀.₁₈Y₁.₈₂} shows field induced SMM behaviour with an anisotropy barrier U_{eff} of 69.3 K. Furthermore, the theoretical magnetic properties of [M₂ᴵᴵᴵLn₂ᴵᴵᴵ(μ₃-OH)₂(*p*-Me-PhCO₂)₆(L)₂] (M = Cr, **1** or Mn, **3**) and their isostructural complexes: [M₂ᴵᴵᴵDy₂ᴵᴵᴵ(μ₃-OH)₂(*p*-Me-PhCO₂)₆(L)₂] (M = Fe, **5** or Al, **7**) are discussed and compared. To understand the experimental observations for this family, DFT and *ab initio* CASSCF + RASSI-SO calculations were performed. The experimental and theoretical calculations suggest that altering the 3dᴵᴵᴵ ions can affect the single-ion properties and the nature and the magnitude of the 3dᴵᴵᴵ–3dᴵᴵᴵ, 3dᴵᴵᴵ–Dyᴵᴵᴵ and Dyᴵᴵᴵ–Dyᴵᴵᴵ magnetic coupling, thus quenching the quantum tunneling of magnetisation (QTM) significantly, thereby improving the SMM properties within this motif. This is the first systematic study looking at variation and therefore role of trivalent transition metal ions, as well as the diamgnetic Alᴵᴵᴵ ion, on slow relaxation of magnetisation within a series of isostructural 3d–4f butterfly compounds.

aInstitute of Inorganic Chemistry, Karlsruhe Institute of Technology, Engesserstrasse 15, 76131 Karlsruhe, Germany. E-mail: annie.powell@kit.edu

bInstitute of Nanotechnology, Karlsruhe Institute of Technology, Postfach 3640, 76021 Karlsruhe, Germany

cIITB-Monash Research Academy, Indian Institute of Technology Bombay, Powai, Mumbai 400076, India. E-mail: rajaraman@chem.iitb.ac.in

† Electronic supplementary information (ESI) available. CCDC 1880458, 1880459, 1880460 and 1902469. For ESI and crystallographic data in CIF or other electronic format see DOI: 10.1039/c8sc05362f

Introduction

Recently, combining 3d and 4f metal ions in a molecule to obtain SMMs has become a hot research topic since 3d ions can give rise to stronger magnetic coupling and/or magnetic anisotropy while 4f ions such as Dyᴵᴵᴵ, Tbᴵᴵᴵ, Hoᴵᴵᴵ, contribute large single-ion magnetic anisotropy.[1–3] Through the efforts of several research groups, there is now a rich structural diversity of 3d–4f SMMs.[4] However, it is still a challenge to understand the correlation between the structure and the magnetic properties.

The single-ion anisotropy of a metal ion depends mainly on its coordination geometry and ligand field,[5] while the molecular anisotropy depends on several factors such as ligand field,[6] relative orientation of the individual single-ion easy axes,[7] magnetic coupling, and the structural topology of the magnetic core.[8,9]

It is well-known that the magnetic interactions between the 3d–3d, 3d–4f, and 4f–4f ions in heterometallic clusters are rather complicated to figure out, especially for clusters with high nuclearity. Thus, to better understand the magnetic interactions between 3d and 4f metal ions as well as the effect of magnetic interactions on the SMM behaviour,[10,11] the construction of simple complexes with a limited number of 3d and 4f ions is required in order to elucidate the magneto-structural correlations. A fruitful test-bed system is provided by the tetranuclear "butterfly" motif. There are two possibilities for 3d/4f butterflies, either the 4f metal ions can be in the body positions and the 3d transition metal M ions are at the wingtips (Type I) or the reverse situation where the 4f metal ions are at the wingtips and the transition metal M ions are in the body positions (Type II). There are relatively few examples of the Type

I situation compared with compounds with the Type II motif. The most famous Type I compounds have been reported by the Murray group where the isostructural compounds, $\{M_2^{III}Ln_2^{III}\}$, (M = Co, Cr and Ln = Dy, Tb, Ho) were studied.[12–14] The corresponding $\{Cr_2Ln_2\}$ and $\{Co_2Ln_2\}$ compounds have similar U_{eff} values, but open magnetic hysteresis was only observed for the $\{Cr_2^{III}Ln_2\}$ compounds where the 3d ion is paramagnetic rather than diamagnetic. It was found using *ab initio* calculations that this is the direct result of the cooperative 3d–4f coupling between the Cr^{III} and Ln^{III} ions.

A particularly fruitful test-bed system for Type II is the generic $[M_2^{III}Ln_2^{III}(\mu_3\text{-OH})_2(RCO_2)_6(L)_2]$ coordination cluster. There are many such examples of 3d–4f butterfly compounds in the literature, including an interesting systematic study by Winpenny, McInnes and their co-workers on a family of $\{M_2Ln_2\}$ compounds where M = Mg^{II}, Mn^{III}, Co^{II}, Ni^{II}, and Cu^{II}, Ln = Y^{III}, Gd^{III}, Tb^{III}, Dy^{III}, Ho^{III}, and Er^{III}. The results revealed that the SMM behaviour observed in the Dy- and Er-based systems are intrinsic to the lanthanide ion and the strength of the 3d–4f exchange interaction plays a key role in the nature of the SMM properties observed.[15] For this system, all the metals (M) are bivalent apart from the Mn^{III} analogue. Up to now the equivalent exploration of this type of butterfly system for M = M^{III} has not been available, probably because of the synthetic challenge to vary the M^{III} metal ions. On the other hand, it is straightforward to vary the 4f ion, as shown for (Type II) $\{Fe_2Ln_2\}$ butterflies.[16] We were particularly interested to gauge the effect that changing the electron configuration of the 3d ion has on the magnetic properties, including potential single molecule magnet (SMM) behaviour in a series of compounds incorporating the highly anisotropic Dy^{III} ion. In order to find some clear-cut ground rules, the system should be poised in such a way that the appearance of SMM behaviour allows an easy identification of the "best" choice of 3d configuration to optimise the slow relaxation and therefore SMM properties. With this in mind, and stimulated by our recent work[17] on $\{M_2^{III}Dy_2^{III}\}$, M = Fe and Al, we extended our study on the high spin 3d⁵ (Fe^{III}) to 3d³ (Cr^{III}) and high spin 3d⁴ (Mn^{III}), and also the yttrium diluted $\{Al_2Dy_2\}$ analogue, $\{Al_2Dy_{0.18}Y_{1.82}\}$. This allows us to probe the nature of the $3d^{III}$–$3d^{III}$, $3d^{III}$–$4f^{III}$ and $4f^{III}$–$4f^{III}$ interactions and the effects on SMM behaviour. We have used a combined experimental and theory approach, using detailed *ab initio* calculations to elucidate the observations from bulk susceptibility and magnetisation data in order to explore the cooperativity and nature of any magnetisation relaxation for the complexes **1** $\{Cr_2Dy_2\}$, **3** $\{Mn_2Dy_2\}$, **5** $\{Fe_2Dy_2\}$ and **7** $\{Al_2Dy_2\}$.

Results and discussion

Synthetic description

Reaction of the (3d/Al^{III}), 4f chloride precursors, $HO_2CPh\text{-Me-}p$ and H_2L in the presence of Et_3N in MeOH and MeCN gives a family of isostructural tetrametallic $\{M_2^{III}Ln_2^{III}\}$ clusters. The molecules feature a butterfly core with an $\{M_2^{III}\}$ body and Ln wingtips, of formula $[M_2^{III}Ln_2^{III}(\mu_3\text{-OH})_2(L)_2(O_2CPh\text{-Me-}p)_6]$ (M = Cr, Mn, Fe and Al, Ln = Dy and Y), based on the synthetic method for the previously reported Fe and Al analogues.[17] In

order to figure out the dipolar interaction effect within the $\{Al_2Dy_2\}$, the analogue $\{Al_2Dy_{0.18}Y_{1.82}\}$ was synthesized and magnetic properties were investigated. For the $\{Mn_2^{III}Ln_2\}$-analogue, the 3d chloride precursor is $MnⁱⁱCl_2$, as was the case in the synthesis of $\{Fe_2Dy_2\}$.[17] During the crystallisation process, the Fe^{II} and Mn^{II} were oxidised to Fe^{III} and Mn^{III} *in situ*. We found that it was necessary to reduce the amount of base for the synthesis of $\{Mn_2Ln_2\}$ compared with the Fe^{III} analogue. $M^{III}Cl_3$ was used to synthesise the Cr and Al compounds with the synthesis for the Cr compound being the same as we reported for the Al compound.[17]

Crystal structures

Compounds **1** $\{Cr_2Dy_2\}$, **2** $\{Cr_2Y_2\}$ and **8** $\{Al_2Dy_{0.18}Y_{1.82}\}$ crystallise isomorphously in $C2/c$ with formulae $[Cr_2^{III}Ln_2^{III}(\mu_3\text{-OH})_2(L)_2(O_2CPh\text{-Me-}p)_6]\cdot2MeCN$ (**1** and **2**) $[Al_2^{III}Dy_2^{III}Y_{1.82}(\mu_3\text{-OH})_2(L)_2(O_2CPh\text{-Me-}p)_6]\cdot2MeCN$ (**8**) respectively. The structures are also isomorphous with the previously reported $\{Al_2Dy_2\}$ compound. Compounds **3** $\{Mn_2Dy_2\}$ and **4** $\{Mn_2Y_2\}$ are isomorphous, crystallising in $P\bar{1}$ with formula $[Mn_2^{III}Ln_2^{III}(\mu_3\text{-OH})_2(L)_2(O_2CPh\text{-Me-}p)_6]\cdot2MeOH\cdot2MCN$. The refinement details are listed in Table S1, ESI.†

The molecular structures of the complexes are very similar in all cases and always centrosymmetric, which was also the case for the previously reported **5** $\{Fe_2Ln_2\}$ (Fig. 1 and S1, ESI†).[17] The description of **1** $\{Cr_2Dy_2\}$ is given as representative for the description of the features of the molecular structures. The neutral cluster is composed of 2 Cr^{III}, 2 Dy^{III}, 2 μ_3-OH, and 6p-Me-PhCOOH. All M^{III} ions have an octahedral O6 donor set which was established from the crystal data and through a SHAPE 2.1 analysis.[18–20] The M^{III} ions have deviation values of 0.42, 1.37, 0.80 and 0.49 (Table 1) for complexes **1** $\{Cr_2Dy_2\}$, **3** $\{Mn_2Dy_2\}$, **5** $\{Fe_2Dy_2\}$ and **7** $\{Al_2Dy_2\}$, respectively.

The Dy^{III} ions with an O7N2 donor set were also systematically analysed using SHAPE 2.1 software,[18–20] and are best described as having a distorted spherical capped square antiprism geometry with deviation values of 0.94, 1.20, 1.00 and 1.00 (Table 1) for complexes **1** $\{Cr_2Dy_2\}$, **3** $\{Mn_2Dy_2\}$, **5** $\{Fe_2Dy_2\}$ and **7** $\{Al_2Dy_2\}$, respectively. The high spin Mn^{III} ions in $\{Mn_2Dy_2\}$ show an axial Jahn–Teller elongation along O4–M–O1′ with an elongated octahedral environment typical for this d⁴ metal ion (Mn–O_{eq} range = 1.894(16)–1.972(18) Å, Mn–O_{ax} =
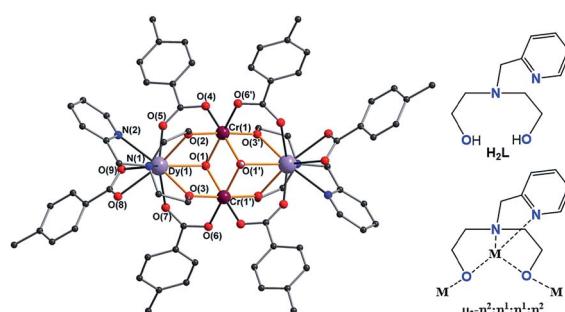

Fig. 1 Structure of compound **1** $\{Cr_2Dy_2\}$ (left), ligand (right upper) and coordination mode of ligand (right lower) in complexes **1**, **3**, **5** and **7**.

Table 1 Continuous shape measurement calculations for the M^{III} and Dy^{III} ions in complexes **1** {Cr$_2$Dy$_2$}, **3** {Mn$_2$Dy$_2$}, **5** {Fe$_2$Dy$_2$} and **7** {Al$_2$Dy$_2$}[a]

	1 {Cr$_2$Dy$_2$}	**3** {Mn$_2$Dy$_2$}	**5** {Fe$_2$Dy$_2$}	**7** {Al$_2$Dy$_2$}
M^{III}	Cr	Mn	Fe	Al
HP	30.21	32.10	31.35	30.31
PPY	25.60	25.69	24.99	25.54
OC	0.42	1.37	0.80	0.49
TPR	14.09	11.78	12.01	13.54
JPPY	29.37	28.75	29.09	29.31

	1 {Cr$_2$Dy$_2$}	**3** {Mn$_2$Dy$_2$}	**5** {Fe$_2$Dy$_2$}	**7** {Al$_2$Dy$_2$}
Ln^{III}	Dy	Dy	Dy	Dy
CSAPR	0.94	1.20	1.00	1.00
TCTPR	1.43	1.25	1.22	1.90
MFF	1.51	1.67	1.47	1.44

[a] HP (D_{6h}) hexagon, PPY (C_{5v}) pentagonal pyramid, OC (C_{4v}) octahedron, TPR (D_{3h}) trigonal prism, JPPY (C_{5v}) Johnson pentagonal pyramid J2, CSAPR (C_{4v}) spherical capped square antiprism, TCTPR (D_{3h}) spherical tricapped trigonal prism, MFF (C_s) muffin.

2.161(16)–2.206 (16) Å (Table 2). The Y analogues were established to be isostructural from the single crystal structure analysis or, in the case of **4**, from the unit cell parameters.

In all cases, there are μ_3-OH hydrogen bonding interactions to lattice solvent molecules but not to other molecules.

Table 2 Selected bonds length (Å) and angles (°) of **1**, **3**, **5** and **7**

|	**1** (Cr^{III})	**3** (Mn^{III})	**5** (Fe^{III})	**7** (Al^{III})
Dy1–O2	2.340 (4)	2.3183 (18)	2.3215 (17)	2.3200 (15)
Dy1–O3	2.326 (4)	2.3651 (15)	2.3416 (16)	2.3308 (16)
Dy1–O7^i	2.430 (4)	2.4311 (18)	2.4332 (17)	2.4046 (16)
Dy1–O1	2.423 (4)	2.3742 (17)	2.3990 (17)	2.4214 (16)
Dy1–O9	2.430 (4)	2.5170 (19)	2.4388 (17)	2.4538 (16)
Dy1–O5	2.402 (5)	2.3713 (16)	2.4434 (17)	2.4212 (16)
Dy1–O8	2.442 (5)	2.3943 (18)	2.4285 (18)	2.4371 (17)
Dy1–N2	2.567 (5)	2.584 (2)	2.566 (2)	2.5640 (19)
Dy1–N1	2.582 (5)	2.628 (2)	2.618 (2)	2.602 (2)
M1–M1^i	3.0659 (2)	3.286 (1)	3.211 (0)	3.024 (1)
Dy1–M1^i	3.4317 (11)	3.376 (1)	3.450 (1)	3.386 (1)
Dy1–M1	3.4404 (11)	3.467 (1)	3.444 (1)	3.383 (1)
M1–O2	1.963 (4)	1.8963 (16)	1.9738 (17)	1.8701 (17)
M1–O4^i	1.969 (4)	2.1610 (16)	1.9944 (17)	1.8875 (17)
M1–O6	1.976 (4)	1.9496 (18)	2.0058 (17)	1.8977 (17)
M1–O3	1.955 (4)	1.8944 (16)	1.9676 (17)	1.8668 (17)
M1–O1	2.002 (4)	1.9727 (16)	2.0584 (17)	1.9496 (17)
M1–O1^i	1.996 (4)	2.2036 (16)	2.0548 (16)	1.9346 (17)
Dy–Dy$_{intra}$	6.150 (4)	6.003 (2)	6.101 (1)	6.055 (1)
Dy–Dy$_{inter}$	7.7708 (5)	10.1349 (2)	7.951 (1)	8.093 (2)
M1–O1–M1^i	100.16 (19)	103.66 (7)	102.65 (7)	102.27 (8)
M1^i–O1–Dy1	101.83 (19)	98.39 (6)	101.28 (7)	101.44 (7)
M1–O1–Dy1	101.30 (16)	101.55 (7)	100.90 (6)	100.85 (7)
M1–O2–Dy1	105.47 (17)	106.03 (7)	106.32 (7)	107.29 (7)
M1^i–O3–Dy1	106.62 (18)	108.46 (7)	106.07 (7)	106.90 (7)

Compounds **1** {Cr$_2$Dy$_2$} and the doped **8** {Al$_2$(Y/Dy)$_2$} are isomorphous to the previously reported compounds **7** {Al$_2$Dy$_2$} and **5** {Fe$_2$Dy$_2$}.[17] There are reasonably strong π–π stacking interactions, with C···C distances down to 3.446 Å, linking the molecules into 2-D sheets. For compound **3** {Mn$_2$Dy$_2$}, there are similarly strong π–π interactions (shortest C···C 3.411 Å) linking the molecules into 1-D chains. Selected bond lengths and angles for the Dy^{III}-containing complexes are listed in Table 2.

Magnetism

Static magnetic studies. Direct-current (dc) magnetic susceptibility studies on complexes **1–4** and **8** were performed on polycrystalline samples in the temperature range 2–300 K, under an applied field (H) of 300 Oe. Magnetisation as a function of applied field was investigated in the field range 0–7 T and at temperatures of 2 and 5 K. The magnetic behaviour of **5** and **6** {Fe$_2$Ln$_2$} (Ln = **5**, Dy and **6**, Y) and **7** {Al$_2$Dy$_2$} were reported previously.[17]

In order to understand how the paramagnetic 3d^{III}-metal affects the magnetic behaviour of the Dy^{III} in the {M$_2^{III}$Dy$_2$}-clusters, we also describe the yttrium diluted {Al$_2$Dy$_2$} compound, {Al$_2$Dy$_{0.18}$Y$_{1.82}$} and the {M$_2$Y$_2$} examples, as we did in the previous study on {Fe$_2$Dy$_2$}.[17] This enables us to indirectly assess the 3d–4f interactions in these examples through comparison of the χT vs. T behaviour of {M$_2$Dy$_2$} with the sum of the contributions for the appropriate {M$_2$Y$_2$} and {Al$_2$Dy$_2$} systems. The dc susceptibility data for all the compounds are summarised in Table S2, ESI.†

Effect of deletion of the 4f contributions in {M$_2$Y$_2$}. The magnetic behaviours for {M$_2$Y$_2$} (M = Cr, **2** and Mn, **4**) are depicted in Fig. 2 and 3. The χT value for {Cr$_2$Y$_2$} (**2**) at room temperature is 3.73 cm^3 K mol^{-1} (consistent with two uncoupled S = 3/2 Cr^{III} ions with g = 2.0; see Table S2, ESI† and Fig. 2) decreasing only slowly until about 10 K, below which it quickly drops to 1.44 cm^3 K mol^{-1}. This suggests antiferromagnetic coupling between the Cr^{III} ions and the fit of the χT plot of **2** {Cr$_2$Y$_2$} using the PHI software[21] gives an antiferromagnetic coupling of $J_{Cr–Cr}$ = −0.49 cm^{-1} for g = 2.0. The molar
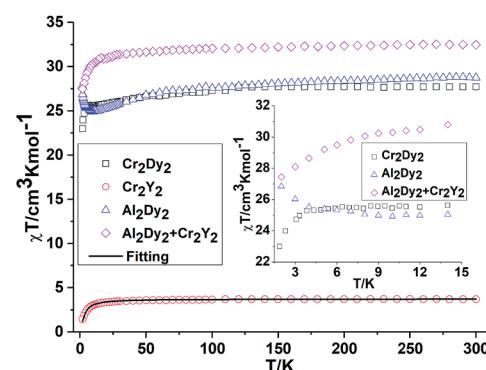
Fig. 2 Temperature dependence of the χT product at 300 Oe for **1** {Cr$_2$Dy$_2$}, **2** {Cr$_2$Y$_2$} (the solid line is the best fit to the experimental data for **2** {Cr$_2$Y$_2$} and **7** {Al$_2$Dy$_2$}). The comparison curves (inset) of {Cr$_2$Dy$_2$} and {Al$_2$Dy$_2$} + {Cr$_2$Y$_2$} along with the curves of **2** {Cr$_2$Y$_2$} and **7** {Al$_2$Dy$_2$} enlarged in the region below 15 K.
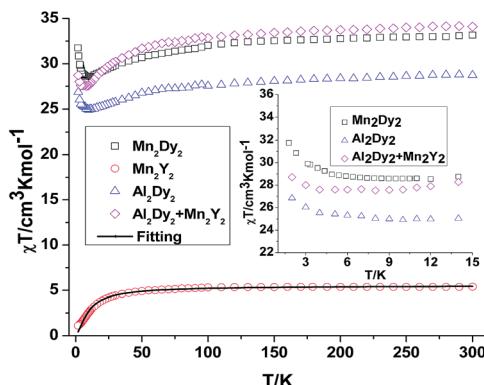
Fig. 3 Temperature dependence of the χT product at 300 Oe for **3** {Mn$_2$Dy$_2$}, **4** {Mn$_2$Y$_2$} (the solid line is the best fit to the experimental data for **4**). The comparison curves (inset) of {Mn$_2$Dy$_2$} and {Al$_2$Dy$_2$} + {Mn$_2$Y$_2$} along with the curves of **4** {Mn$_2$Y$_2$} and **7** {Al$_2$Dy$_2$} enlarged in the region below 15 K.

magnetisation (M) as a function of applied magnetic field at 2 K in the field range 0–7 T does not saturate but does show a value close to the expected saturation value at 7 T for compound **2** {Cr$_2$Y$_2$} of 6.95 μ_B, which is in line with the result that the exchange between these two Cr^{III} ions is fairly weak (Fig. S2, ESI†).

For {Mn$_2$Y$_2$} (**4**), the χT value at room temperature is 5.38 cm^3 K mol^{-1} which is lower than what is expected for two uncoupled $S = 2$ Mn^{III} ions with $g = 2.0$ (see Table S2† and Fig. 3). The χT value decreases slowly down to about 30 K below which it decreases rapidly to reach 1.10 cm^3 K mol^{-1} at 2 K (Fig. 3). This could be due to antiferromagnetic coupling or significant single ion anisotropy. The χT plot of **4** {Mn$_2$Y$_2$} was also fitted using the PHI software[21] and an antiferromagnetic coupling with $J_{Mn-Mn} = -1.00$ cm^{-1} and $g = 1.92$ was found – *i.e.* about twice as strong as for the Cr^{III} compound and in line with the fact that Mn^{III} has four rather than three unpaired electrons. The stronger Mn–Mn AF coupling is more likely to reflect the single electron now in the 3d$_{z^2}$ Mn^{III} orbital, this orbital being empty for Cr^{III}. The Jahn–Teller axis of Mn (and thus this orbital) points towards one of the bridging OH groups, so for each Mn–OH–Mn bridge, one of the two Mn–O interactions involves a 3d orbital with an unpaired electron in it, while for Cr both the 3d orbitals are empty. The reduced magnetisation M–H plots of **4** {Mn$_2$Y$_2$} show a crossover feature at about 2 T (Fig. S2†), which is likely to be the result of significant anisotropy, as previously observed in a {Co$^{II}_2$Y$_2$} compound.[15]

Inclusion of 4f contribution in {M$_2$Dy$_2$}. For complex **1**, {Cr$_2$Dy$_2$}, as shown in Fig. 2, at 300 K, the experimental χT value is 27.70 cm^3 K mol^{-1}, which is much lower than the expected value of 32.09 cm^3 K mol^{-1} for two spin-only Cr^{III} ions ($S = 3/2$, $g = 2$, $C = 1.875$ cm^3 K mol^{-1}) and two Dy^{III} ions ($S = 5/2$, $L = 5$, ^{6}H$_{15/2}$, $g = 4/3$, $C = 14.17$ cm^3 K mol^{-1}). The χT product remains almost constant over the whole temperature range, reaching a minimum value of 23.08 cm^3 K mol^{-1} at 2 K. This behaviour is typically observed when both antiferromagnetic interactions between magnetic ions and the thermal depopulation of the

Dy^{III} excited states are operative.[22,23] In order to probe the interaction between Cr^{III} and Dy^{III} ions in complex **1** {Cr$_2$Dy$_2$}, the χT *vs.* T curves for {Cr$_2$Dy$_2$} and the addition of {Al$_2$Dy$_2$} data to that of {Cr$_2$Y$_2$} in [{Al$_2$Dy$_2$} + {Cr$_2$Y$_2$}] can be compared (Fig. 2). This makes it possible to gauge any cooperative effects within the **1** {Cr$_2$Dy$_2$} data by seeing whether "the sum of the parts" *i.e.* addition of the curves for **2** {Cr$_2$Y$_2$} and **7** {Al$_2$Dy$_2$}, differs from the observed data for the actual **1** {Cr$_2$Dy$_2$} compound, since the {Al$_2$Dy$_2$} + {Cr$_2$Y$_2$} data effectively 'deletes' the contribution of the Cr–Dy interaction.

As shown in the inset of Fig. 2, the χT value at low temperature for {Cr$_2$Dy$_2$} is lower than the corresponding values for [{Cr$_2$Y$_2$} + {Al$_2$Dy$_2$}], indicating a contribution from antiferromagnetic coupling between the Cr^{III} and Dy^{III} ions.

For complex **3** {Mn$_2$Dy$_2$}, the room temperature χT value of 33.16 cm^3 K mol^{-1} is in good agreement with the expected value of 33.17 cm^3 K mol^{-1} for two uncoupled Mn^{III} ions ($S = 2$, $g = 2.0$, $C = 2.50$ cm^3 K mol^{-1}) and two uncoupled Dy^{III} ions ($S = 5/2$, $L = 5$, ^{6}H$_{15/2}$, $g = 4/3$, $C = 14.17$ cm^3 K mol^{-1}). As the temperature is lowered, the χT product gradually decreases until 15 K, below which it increases to 28.03 cm^3 K mol^{-1} at 2 K. The decrease in χT at higher temperatures can be attributed to the depopulation of the excited states of the Dy^{III} ions, whereas the increase at lower temperature suggests significant ferromagnetic interactions between the Mn^{III} and Dy^{III} ions. Modelling the **3** {Mn$_2$Dy$_2$} data by addition of the curves for **4** {Mn$_2$Y$_2$} and **7** {Al$_2$Dy$_2$}, as shown in the inset of Fig. 3, reveals that the interactions between Mn^{III} and Dy^{III} ions are ferromagnetic.

The field dependence of the magnetisation of **1** {Cr$_2$Dy$_2$} and **3** {Mn$_2$Dy$_2$} were performed at fields ranging from 0 to 7 T at 2 and 5 K. At higher fields, M increases linearly without clear saturation to ultimately reach 16.85 μ_B ($H = 7$ T, at 2 K) for **1** {Cr$_2$Dy$_2$} and 11.90 μ_B ($H = 7$ T, at 2 K) for **3** {Mn$_2$Dy$_2$}. The lack of saturation on a single master curve of M *vs.* H data for both complexes suggests the presence of magnetic anisotropy (Fig. S2†).

Dynamic susceptibility studies. To probe potential slow magnetisation relaxation, ac magnetic measurements were carried out for **1** {Cr$_2$Dy$_2$}, **3** {Mn$_2$Dy$_2$}, and **8** {Al$_2$Dy$_{0.18}$Y$_{1.82}$}.

{Cr$_2$Dy$_2$} 1. No out-of-phase signal (χ'') was observed even after a static dc field (Fig. S3†) was applied, indicating the absence of SMM behaviour within the measurement parameters of the SQUID.

{Mn$_2$Dy$_2$} 3. Both the in-phase (χ') and out-of-phase (χ'') susceptibilities display frequency and temperature dependence, signalling the blocking of the magnetisation due to an anisotropy barrier (Fig. 4 and S4, ESI†). The χ'' *vs.* ν plots were observed in fields up to 1000 Oe (Fig. S5, ESI†), further suggesting that QTM is inefficient in this system. A plot of χ'' *vs.* ν isotherms (Fig. 4, lower right), reveals frequency dependent maxima down to 1.8 K. From these data, Cole–Cole plots (Fig. 5, left) were constructed and fitted to a generalized Debye model using CC-fit[24] to determine α values and relaxation times (τ_0) in the temperature range 1.8–2.4 K. The plots reveal relatively symmetrical semicircles, indicating a single relaxation process, with α values ranging from 0.067–0.093, indicating a narrow
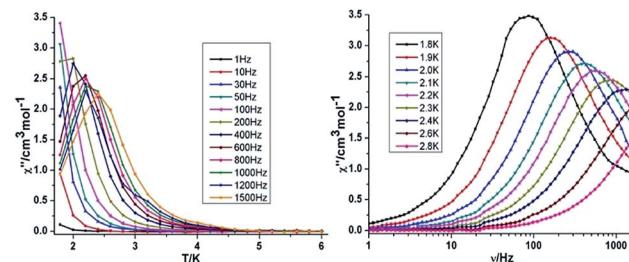
Fig. 4 Temperature (left) and frequency (right) dependence under zero dc field of the out-of-phase (χ'') for compound **3** {Mn$_2$Dy$_2$}.
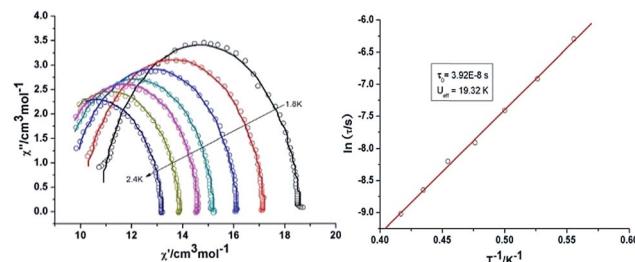
Fig. 5 Cole–Cole plots at indicated temperature (left) and τ vs. T^{-1} plot in zero dc field (right) for **3** {Mn$_2$Dy$_2$}.

distribution of relaxation times within this single relaxation process. From the frequency-dependent behaviour, it was found that the relaxation follows a thermally activated mechanism from 1.8–2.4 K and plots of $\ln(\tau)$ vs. $1/T$ are linear (Fig. 5, right). Fitting to the Arrhenius law [$\tau = \tau_0 \exp(U_{eff}/k_BT)$] afforded values of $U_{eff} = 19.32$ K and $\tau_0 = 5.64 \times 10^{-8}$ s. This result indicates a barrier to thermal relaxation, with the pre-exponential factor consistent with the expected value for an SMM of between 10^{-6}–10^{-11}.[25] The energy barrier is comparable with that of the previously reported [NMe$_4$]$_2$[Mn$_2^{III}$Dy$_2^{III}$(tmp)$_2$(O$_2$CMe$_3$)$_4$(NO$_3$)$_4$]· 2MeCN·0.5H$_2$O[26] (15 K) and [Et$_3$NH]$_2$[Mn$_2^{III}$Ln$_2^{III}$(μ_3-O)$_2$(O$_2$C^{t}Bu)$_{10}$] (29 K) complexes.[15] The relaxation time, τ, does not become temperature independent at low temperature down to 1.8 K, indicating the absence of a pure quantum regime down to 1.8 K (when the tunnelling rate becomes faster than the activated relaxation). Upon application of a static dc field, a technique used to reduce quantum tunnelling effects, no significant shift in the maximum position of the temperature in the χ'' vs. ν plots were observed in fields up to 1000 Oe (Fig. S5, ESI†), further suggesting that QTM is inefficient in this system.

{Al$_2$Dy$_{0.18}$Y$_{1.82}$} **8**. Under zero dc field, quantum tunnelling of the magnetisation (QTM) was observed, preventing the occurrence of clear peaks for **8** (Fig. S6, ESI†) which can be compared with the situation found for our previously reported complex **7** {Al$_2$Dy$_2$}[17] where typical SMM behaviour could be observed without application of a dc field with $U_{eff} = 38.7$ K and $\tau_0 = 1.06 \times 10^{-6}$ s. In ref. 17, we specifically targeted the "Fe(III) knockout" for the {Fe$_2$Dy$_2$} compound through replacement with diamagnetic Al(III) in order to investigate the cooperativity between the Dy and Fe ions within this butterfly system. Since we were also able to investigate this system using ^{57}Fe

Mössbauer spectroscopy, we could also gauge the influence of the strongly antiferromagnetically coupled central dinuclear Fe$_2$ unit on the uniaxial anisotropy directions of the wingtip Dy(III) ions through a consideration of the multiple hyperfine interactions which could be observed. An important conclusion from this work was the major roles played by the local magnetic fields of the ions involved. By deleting Fe(III) from the compound we could suggest that the uniaxial directions of the magnetic anisotropy on the wingtip Dy(III) ions changed orientation once the influence of the Fe(III) ions was taken away. This helps to explain the rather good SMM behaviour of the pure {Al$_2$Dy$_2$} compound. Now it seems that reducing the Dy(III) influence within the {Al$_2$Dy$_2$} system through dilution with diamagnetic Y(III) leads to a "loss of direction" for the dipolarly coupled Dy(III) ions and a breakdown in suppression of QTM for **8** {Al$_2$Dy$_{0.18}$Y$_{1.82}$}. Thus, only through application of a dc field to **8** {Al$_2$Dy$_{0.18}$Y$_{1.82}$} could clear peaks be observed in the out of phase (χ'') data (Fig. S7, ESI†), indicating field-induced SMM behaviour. Since this behaviour is observed only upon application of a static field we can attribute it to suppression of the quantum tunnelling of the magnetisation between sublevels, which is very fast under zero dc field and is observed when the single 4f ion properties become important (achieved here through dilution) and the geometry of the ligand field is sub-optimal for inducing a strong uniaxial, i.e. Ising type of anisotropy. Such activity is known for many lanthanide SMMs.[27–29]

Temperature and frequency dependent in phase (χ') and out of phase (χ'') ac measurements were performed using an applied dc field of 1000 Oe (Fig. 6 and S8, ESI†). This field was chosen to allow for comparisons with previously reported systems. A fitting of the data extracted from the frequency dependent out of phase (χ'') signals using the Arrhenius equation ($\tau = \tau_0 \exp(U_{eff}/k_BT)$) gives an energy barrier of $U_{eff} = 69.26$ K and pre-exponential factor of $\tau_0 = 1.18 \times 10^{-7}$ s (Fig. S9, ESI†). Cole–Cole plots (χ'' vs. χ') for the temperature range 3.5–9.0 K (Fig. S9, ESI†) can be fitted for a single relaxation process using the Debye model to give α parameters in the range 0.14–0.28, indicating a wider distribution of relaxation times than seen for the non-diluted compound **7** {Al$_2$Dy$_2$}. This result indicates that the dipolar interaction between the two distant wingtip Dy^{III} ions plays a key role in suppressing the QTM.[30] The comparison data are summarized in Table 3.

Theoretical studies. The magnetic properties of complexes **1** {Cr$_2$Dy$_2$}, **3** {Mn$_2$Dy$_2$}, **5** {Fe$_2$Dy$_2$} and **7** {Al$_2$Dy$_2$} were studied using
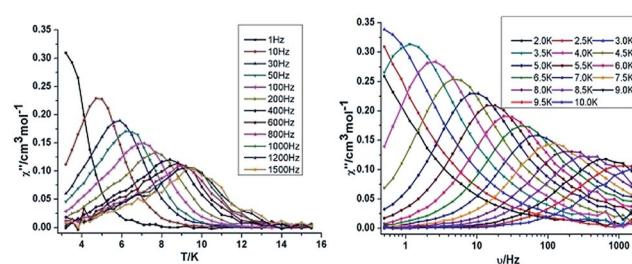
**Fig. 6** Temperature (left) and frequency (right) dependence under 1000 Oe dc field of the out-of-phase (χ'') for compound **8** {Al$_2$Dy$_{0.18}$Y$_{1.82}$}.

Table 3 The selected parameters for complexes **1** {Cr$_2$Dy$_2$}, **3** {Mn$_2$Dy$_2$}, **5** {Fe$_2$Dy$_2$}, **7** {Al$_2$Dy$_2$} and **8** {Al$_2$Dy$_{0.18}$Y$_{1.82}$}

	3d–3d	3d–Dy	Dy–Dy	SMMs (field/Oe)
1 {Cr$_2$Dy$_2$}	AF	AF	F	No
3 {Mn$_2$Dy$_2$}	AF	F	F	Yes (0)
5 {Fe$_2$Dy$_2$}	AF	AF	F	Yes (1000)
7 {Al$_2$Dy$_2$}	—	—	F	Yes (0)
8 {Al$_2$Dy$_{0.18}$Y$_{1.82}$}	—	—	F	Yes (1000)

ab initio CASSCF[31] + RASSI-SO[32] calculations. SINGLE_ANISO[33–36] routine was used for the anisotropy calculation of the individual paramagnetic ions followed by POLY_ANISO routine, which uses the Lines model to fit the susceptibility plots.[37] First, we explore the single ion relaxation mechanism for each Dy^{III} ion, followed by the discussion of the polynuclear system where all single-ion anisotropy and the magnetic exchange constants are employed to develop a description of the relaxation mechanism(s) for the exchange coupled system.

Single-ion magnetic anisotropy of complexes 1 {Cr$_2$Dy$_2$}, 3 {Mn$_2$Dy$_2$}, 5 {Fe$_2$Dy$_2$} and 7 {Al$_2$Dy$_2$}. In complexes **1** {Cr$_2$Dy$_2$}, **3** {Mn$_2$Dy$_2$} and **5** {Fe$_2$Dy$_2$}, we have explored the anisotropy of all the paramagnetic ions (Cr^{III}, Mn^{III}, Fe^{III} and Dy^{III}). In complex **7** {Al$_2$Dy$_2$}, only two paramagnetic Dy^{III} ions are present. Thus we have explored the anisotropy of Dy^{III} ions for both centres in complex **7** {Al$_2$Dy$_2$}. The calculated anisotropic *g* values for complexes **1** {Cr$_2$Dy$_2$}, **3** {Mn$_2$Dy$_2$}, **5** {Fe$_2$Dy$_2$} and **7** {Al$_2$Dy$_2$} (for KD1 and KD2) are listed in Tables 4 and S3 (ESI†) and their anisotropy orientations are shown in Fig. 7.

The energy gap between the ground to first-excited state KDs is found to be 27.0 cm^{-1} (33.9 cm^{-1}), 50.2 cm^{-1} (50.2 cm^{-1}), 39.9 cm^{-1} (44.0 cm^{-1}), 47.0 cm^{-1} (43.5 cm^{-1}), for Dy1 (Dy2) in complexes **1** {Cr$_2$Dy$_2$}, **3** {Mn$_2$Dy$_2$}, **5** {Fe$_2$Dy$_2$} and **7** {Al$_2$Dy$_2$} respectively (see Table 4). For complex **3** {Mn$_2$Dy$_2$}, both Dy1 and Dy2 are equivalent and therefore the ground to first excited state gap and the *g*-anisotropies are the same while in other cases, both the anisotropy and the gaps are different for the Dy1 and Dy2 ions. In particular, the ground to first excited state energy gaps are significantly larger for complexes **3** {Mn$_2$Dy$_2$}
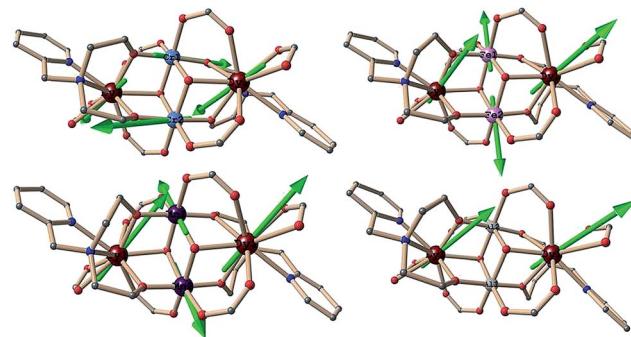
Fig. 7 The directions of the local anisotropy axes in the ground Kramers doublet on each paramagnetic metals site (green solid line) in complexes **1** {Cr$_2$Dy$_2$} upper left, **3** {Mn$_2$Dy$_2$} lower left, **5** {Fe$_2$Dy$_2$} upper right and **7** {Al$_2$Dy$_2$} lower right.

and **7** {Al$_2$Dy$_2$}, while it is computed to be slightly smaller for complex **5** {Fe$_2$Dy$_2$} (Dy1) and much smaller for complex **1** {Cr$_2$Dy$_2$}. Since the energy gap is correlated to the crystal-field splitting energy, this suggests relatively weaker splitting of the m_J levels in **1** {Cr$_2$Dy$_2$} compared to complexes **3** {Mn$_2$Dy$_2$}, **5** {Fe$_2$Dy$_2$} and **7** {Al$_2$Dy$_2$}.

SHAPE 2.1 analysis[18–20] yields a Dy$_{Mn}$ > Dy$_{Fe}$ ∼ Dy$_{Al}$ > Dy$_{Cr}$ trend for the distortion of Dy^{III} ions with respect to the idealised spherical-capped square anti-prismatic geometry and this trend matches with the computed energy gap between ground to first excited state.

The LoProp computed charges[38] obtained from CASSCF calculations for complexes **1** {Cr$_2$Dy$_2$}, **3** {Mn$_2$Dy$_2$}, **5** {Fe$_2$Dy$_2$} and **7** {Al$_2$Dy$_2$} are shown in Fig. 8. For the Dy^{III} ion, the oblate anisotropy ellipsoid means that the density is expected to lie along the plane with the least repulsion. The charge on the μ-alkoxo and μ$_3$-OH are found to be very large in all four cases as they are connected to the trication which tend to polarise the oxygen atom charges significantly. Thus the oblate density lies perpendicular to this direction and the g_{zz} axis lies along the O–Dy–O direction where the oxygen atoms possess the largest negative charges[39,40] In complex **1** {Cr$_2$Dy$_2$}, the g_{zz} axis lies in the direction defined by the oxygen atom of one of the

Table 4 *Ab initio* computed ground state *g*-tensors ($g_{x,y,z1}$), and first excited *g*-tensors ($g_{x,y,z2}$) along with energy separation between ground to first excited state and angle between ground to first excited KDs for both Dy^{III} centres in complexes **1** {Cr$_2$Dy$_2$}, **3** {Mn$_2$Dy$_2$}, **5** {Fe$_2$Dy$_2$} and **7** {Al$_2$Dy$_2$}

		Dy1	$E_{KD1} - E_{KD2}$ (cm^{-1})	Angle	Dy2	$E_{KD1} - E_{KD2}$ (cm^{-1})	Angle
1 {Cr$_2$Dy$_2$}	g_{x1}/g_{x2}	0.28/0.22	27.0	21.8	0.18/0.10	33.9	20.4
	g_{y1}/g_{y2}	0.47/0.45			0.30/0.26		
	g_{z1}/g_{z2}	18.13/18.10			18.67/17.90		
3 {Mn$_2$Dy$_2$}	g_{x1}/g_{x2}	0.13/1.78	50.2	52.1	0.13/1.78	50.2	52.2
	g_{y1}/g_{y2}	0.36/5.93			0.36/5.92		
	g_{z1}/g_{z2}	19.35/12.16			19.34/12.16		
5 {Fe$_2$Dy$_2$}	g_{x1}/g_{x2}	0.25/1.26	39.9	25.4	0.18/0.88	44.0	17.3
	g_{y1}/g_{y2}	0.47/1.40			0.35/0.97		
	g_{z1}/g_{z2}	18.01/15.18			18.09/15.79		
7 {Al$_2$Dy$_2$}	g_{x1}/g_{x2}	0.00/1.02	47.0	35.9	0.00/0.70	43.5	28.3
	g_{y1}/g_{y2}	0.00/1.62			0.00/0.98		
	g_{z1}/g_{z2}	19.05/16.56			19.00/16.98		
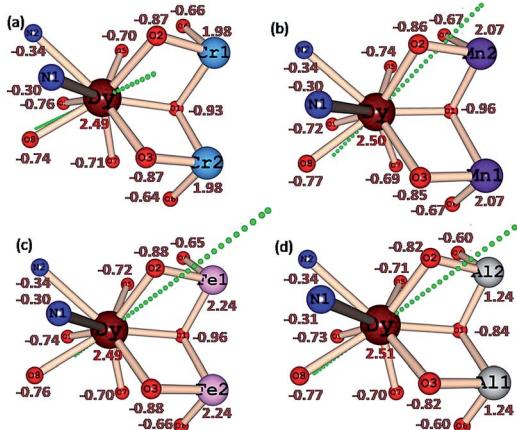
Fig. 8 *Ab initio* computed LoProp charges on the metal atoms and donor atoms of complexes (a) 1 $\{Cr_2Dy_2\}$, (b) 3 $\{Mn_2Dy_2\}$, (c) 5 $\{Fe_2Dy_2\}$ and (d) 7 $\{Al_2Dy_2\}$ (note: because of identical charges on the other half side, we have only shown here one side of the molecule).

carboxylates and the μ-alkoxo oxygen connected to the Cr^{III} ion. While this is found to be similar for complexes 1 $\{Cr_2Dy_2\}$, 3 $\{Mn_2Dy_2\}$, 5 $\{Fe_2Dy_2\}$ and 7 $\{Al_2Dy_2\}$, clearly there are structural variations. For example, the Cr–O (alkoxo) bridging distance is 1.963(4) Å, while in complex 3 $\{Mn_2Dy_2\}$, the Mn–O distance is much shorter (1.896(16) Å) in line with the Jahn–Teller distortion. A shorter bond distance is expected to lead to a greater polarisability of the oxygen and resulting the g_{zz} aligning closest to the μ-alkoxo oxygen with a deviation of only 18°. This is much smaller compared to the case in complex 1 $\{Cr_2Dy_2\}$ (25°). This significant variation in the orientation of the g_{zz} axis caused by the electronic structure of the trication at the body of the butterfly apparently leads to the variation in the ground-state to excited-state gaps. A similar scenario is noted also for complexes 5 $\{Fe_2Dy_2\}$ and 7 $\{Al_2Dy_2\}$, where the ground state g_{zz} axis is found to align along the μ-alkoxo oxygen atom (with deviations of 18.5° for 5 $\{Fe_2Dy_2\}$ and 15.4° for complex 7 $\{Al_2Dy_2\}$). Another important result from the analysis of the charges concerns the charge found at the equatorial position of the Dy^{III} ion, as this is reflected in the transverse anisotropy. For complex 7 $\{Al_2Dy_2\}$, significant reduction of charge on the μ_3-OH group lying in the equatorial plane is noted and this leads to a drastic reduction of transverse anisotropy at −0.84 in 7 $\{Al_2Dy_2\}$ rather than −0.93 in 1 $\{Cr_2Dy_2\}$ or −0.96 in 3 $\{Mn_2Dy_2\}$ and 5 $\{Fe_2Dy_2\}$.

In all the complexes, $m_J = \pm15/2$ is found to be stabilized as the ground state (see Fig. S10, ESI†). This can be attributed to the stronger axial interactions compared to transverse interactions. However, significant transverse anisotropy is present for the ground state KD of complexes 1 $\{Cr_2Dy_2\}$ and 5 $\{Fe_2Dy_2\}$ g_{xx} = 0.28/0.18, g_{yy} = 0.47/0.30, g_{zz} = 18.13/18.67 for Dy1/Dy2 of complex 1 $\{Cr_2Dy_2\}$ and g_{xx} = 0.25/0.18, g_{yy} = 0.47/0.35, g_{zz} = 18.01/18.09 for Dy1/Dy2 of complex 5 $\{Fe_2Dy_2\}$ (Table 4), as a result of the strong mixing of the $m_J = \pm15/2$, $\pm13/2$, $\pm11/2$ and $\pm9/2$ states (see Fig. S10, ESI†). The transverse components for both the complexes are found to be larger for Dy1, and the effect on the measured χT values for both compounds, and

in particular for the $\{Cr_2Dy_2\}$ one, is a substantial decrease in the value expected considering the summation of the Y and Al analogues with the deleted 4f/3d contributions respectively. This at first sight surprising reduction in the χT value has also been observed for a recently reported $\{Cr_2Dy_3\}$ system[41] where this was attributed to the changes in the anisotropies of the Dy(III) ions. It should also be noted that the magnetisation plots for the $\{Cr_2Y_2\}$ compound indicate that the contribution of the coupled Cr(III) ions is far from isotropic in nature.

In complexes 3 $\{Mn_2Dy_2\}$ and 7 $\{Al_2Dy_2\}$, the mixing of KD1 with KD2 is relatively smaller compared to the two complexes 1 $\{Cr_2Dy_2\}$ and 5 $\{Fe_2Dy_2\}$ because of the larger energy separation between them. Significant axial anisotropy is present for the ground state KD of complex 3 $\{Mn_2Dy_2\}$. A clear Ising nature is observed for the Dy^{III} ions in complex 3 $\{Mn_2Dy_2\}$ (g_{xx} = 0.13/0.13, g_{yy} = 0.36/0.36, g_{zz} = 19.35/19.34 for Dy1/Dy2) and even more markedly in complex 7 $\{Al_2Dy_2\}$ (g_{xx} = 0.00/0.00, g_{yy} = 0.00/0.00, g_{zz} = 19.05/19.00 for Dy1/Dy2) see Table 4.

To analyse the various possible relaxation processes associated with the single-ion Dy^{III} anisotropy, the mechanisms of the magnetic relaxation were computed and these are shown in Fig. S10, ESI†.

In complexes 1 $\{Cr_2Dy_2\}$ and 5 $\{Fe_2Dy_2\}$, the ground state tunnelling probability is large for the Dy1 ion (1.2×10^{-1} μ_B). For the Dy ions in the other compounds, the ground state tunnelling probability is found to be smaller (5.0×10^{-2} to 8.8×10^{-2} μ_B). In complexes 1 $\{Cr_2Dy_2\}$ and 5 $\{Fe_2Dy_2\}$, the tunnelling probability at the single ion level in the ground state is larger than in 3 $\{Mn_2Dy_2\}$ and 7 $\{Al_2Dy_2\}$ and the calculations predict the absence of SMM behaviour. This is in accord with the experimental measurements. If we consider relaxation processes beyond those of the single-ion, then factors such as Dy^{III}–Dy^{III} exchange coupling may play a role in quenching the observed QTM. Therefore, the Dy^{III}–Dy^{III}, Dy^{III}–$3d^{III}$ and $3d^{III}$–$3d^{III}$ exchange couplings were taken into account using the POLY_ANISO suite. These gave the $3d^{III}$ single ion isotropic g-tensors (see Table S3 in ESI†) which have values too small to significantly influence the magnetic anisotropy of the Dy^{III} centres apart from for complex 3 $\{Mn_2Dy_2\}$ where the single-ion zero-field splitting, D, values of the Mn^{III} ions are relatively large at −3.35 cm⁻¹, see Table S3 in ESI†.

Mechanism of magnetic relaxation (polynuclear paradigm). As explained in the earlier section, the single ion Dy^{III} anisotropy and the postulated mechanism of relaxation do not fully rationalize the observation of slow magnetic relaxation in complexes 1 $\{Cr_2Dy_2\}$, 3 $\{Mn_2Dy_2\}$, 5 $\{Fe_2Dy_2\}$ and 7 $\{Al_2Dy_2\}$. To gain insights into the mechanism of the exchange interaction a comprehensive mechanism needs to be developed, incorporating the exchange coupling between the paramagnetic centres. This has been performed using the POLY_ANISO program,[37] which employs the Lines model to fit the experimental susceptibility data using the *ab initio* computed parameters of the Dy^{III}/$3d^{III}$ single ion. The exchange Hamiltonian adopted for complexes 1 $\{Cr_2Dy_2\}$, 3 $\{Mn_2Dy_2\}$, 5 $\{Fe_2Dy_2\}$ and 7 $\{Al_2Dy_2\}$ are shown below along with the exchange topology diagram in Fig. 9a.

$$\widehat{H}_{ex} = -\sum_{i=1}^{3} J_i S_i S_{i+1} \qquad (1)$$

Here, $J_i = J_i^{exch}$; *i.e.* J_i are the fitted J_i^{exch} parameters; this describes the interaction between all the neighbouring metal centres. We have employed three exchange interactions ($3d^{III}$–$3d^{III} = J_1$, Dy^{III}–$3d^{III} = J_2$ and Dy^{III}–$Dy^{III} = J_3$, see Fig. 9a) for these four complexes. The estimated exchange coupling parameters are shown in Table 5. The best fit obtained using POLY_ANISO for all four complexes are found to be in good agreement with the experimental plots (see Fig. 9b–e for complexes 1 {Cr$_2$Dy$_2$}, 3 {Mn$_2$Dy$_2$}, 5 {Fe$_2$Dy$_2$} and 7 {Al$_2$Dy$_2$}, respectively).

For complexes 1 {Cr$_2$Dy$_2$}, 3 {Mn$_2$Dy$_2$} and 5 {Fe$_2$Dy$_2$}, magnetic interactions between the transition metals (J_1) are found to be antiferromagnetic in nature with complex 5 {Fe$_2$Dy$_2$} having the largest magnitude of J_1 followed by complex 3 {Mn$_2$Dy$_2$} and complex 1 {Cr$_2$Dy$_2$}. To ascertain the J_1 values independently, DFT calculations were performed on {Cr$_2$La$_2$} and {Mn$_2$La$_2$} models and these values reproduce the sign as well as the magnitude trend for the J_1 interaction. For complexes 1 {Cr$_2$Dy$_2$} and 5 {Fe$_2$Dy$_2$}, the magnetic interaction between Dy–$3d^{III}$ (J_2) is found to be antiferromagnetic whereas for complex 3 {Mn$_2$Dy$_2$}, it is found to be ferromagnetic in nature. All these values are in accord with the earlier literature reports.[40,42] The weak Cr^{III}–Cr^{III} (J_1) interaction in complex 1 {Cr$_2$Dy$_2$} causes the relaxation to occur *via* the ground state with very high QTM probability.

For complexes 1 {Cr$_2$Dy$_2$} and 5 {Fe$_2$Dy$_2$}, the tunnelling (Δ_{tun}) parameters of the exchange coupled ground state are

Table 5 Magnetic exchange interactions (cm^{-1}) between magnetic ions in 1 {Cr$_2$Dy$_2$}, 3 {Mn$_2$Dy$_2$}, 5 {Fe$_2$Dy$_2$} and 7 {Al$_2$Dy$_2$}. zJ is a cluster–cluster interaction

Complex		J_1	J_2	J_3	zJ	J_1 (DFT)
		J values (Lines model)		
1 {Cr$_2$Dy$_2$}	J_{Tot}	−0.65	−1.15	0.405	−0.045	−0.81
	J_{Exc}	−0.50	−0.80	0.370		
	J_{Dip}	−0.15	−0.35	0.035		
3 {Mn$_2$Dy$_2$}	J_{Tot}	−3.20	0.15	0.035	—	−2.10
	J_{Exc}	−2.10	0.09	−0.001		
	J_{Dip}	−1.10	0.06	0.036		
5 {Fe$_2$Dy$_2$}	J_{Tot}	−4.20	−0.12	0.060	—	−4.92
	J_{Exc}	−3.00	−0.05	0.025		
	J_{Dip}	−1.20	−0.07	0.035		
7 {Al$_2$Dy$_2$}	J_{Tot}	—	—	0.049	—	—
	J_{Exc}	—	—	0.025		
	J_{Dip}	—	—	0.024		

computed to be large ($\leq 4.3 \times 10^{-3}$ and $\leq 2.1 \times 10^{-4}$ respectively, see Fig. 10a and c respectively, see Fig. S11 in ESI† for low lying exchange spectra for complexes 1 {Cr$_2$Dy$_2$}, 3 {Mn$_2$Dy$_2$}, 5 {Fe$_2$Dy$_2$} and 7 {Al$_2$Dy$_2$}), whereas for complexes 3 {Mn$_2$Dy$_2$} (6.0×10^{-6}, see Fig. 10b) and 7 {Al$_2$Dy$_2$} (3.6×10^{-6}, see Fig. 10d) the same is computed to be very small. Thus in complex 1 {Cr$_2$Dy$_2$}, the magnetic relaxation occurs *via* the ground state. In complex 3 {Mn$_2$Dy$_2$}, the first excited state possesses relatively high tunnel splitting ($\Delta_{tun} = 1.0 \times 10^{-5}$ cm^{-1}) suggesting relaxation

Fig. 9 (a) Magnetic exchange pathways in complexes 1 {Cr$_2$Dy$_2$}, 3 {Mn$_2$Dy$_2$}, 5 {Fe$_2$Dy$_2$} and 7 {Al$_2$Dy$_2$}. (b–e) Best fit for χT vs. T obtained using POLY_ANISO for complexes 1 {Cr$_2$Dy$_2$}, 3 {Mn$_2$Dy$_2$}, 5 {Fe$_2$Dy$_2$} and 7 {Al$_2$Dy$_2$}, respectively.
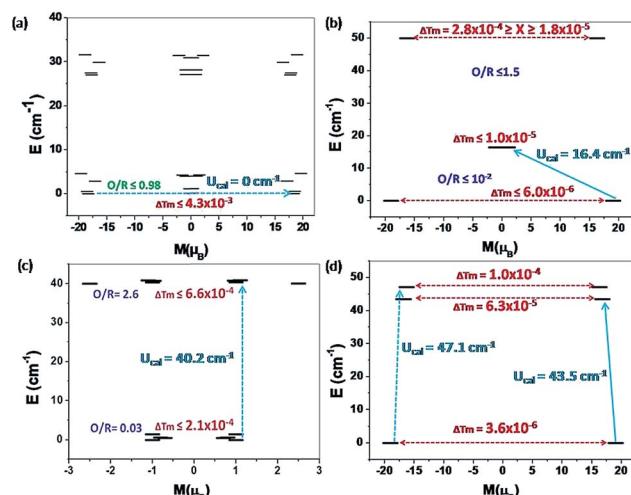
Fig. 10 The *ab initio* POLY_ANISO computed magnetisation blocking barrier for complexes (a) 1 {Cr$_2$Dy$_2$}, (b) 3 {Mn$_2$Dy$_2$}, (c) 5 {Fe$_2$Dy$_2$} and (d) 7 {Al$_2$Dy$_2$}. The x-axis indicates the magnetic moment of each state along main magnetic axis of Dy ions, while y-axis denotes the energy of the respective states. The thick black line indicates the Kramer's doublets as a function of computed magnetic moment. The indigo colour shows the possible pathway *via* Orbach/Raman relaxation. The dotted red lines represent the presence of QTM/TA-QTM between the connecting pairs. The numbers provided are the mean absolute value for the corresponding matrix element of transition magnetic moment. A thick cyan coloured arrow shows the zero field relaxation whereas a dotted cyan coloured arrow shows relaxation in an applied external field.

via the first excited state with U_{cal} value of 16.4 cm^{-1} (see Fig. 10b). This picture is consistent with the experimental data where a relaxation process is observed with a barrier height of 13.5 cm^{-1} (U_{eff}). For complex **5** {Fe$_2$Dy$_2$}, the tunnelling probability of the exchange coupled ground state is found to be large which suggests a possible relaxation pathway *via* the ground state.

Other excited states are found to be below 1.3 cm^{-1} so applying an external magnetic field can overcome this energy barrier and relaxation can occur through the next higher excited state with a barrier height of 40.2 cm^{-1}. This picture is consistent with the experimental data, where in the presence of an external magnetic field relaxation occurs through an excited state with a barrier height of 11.3 cm^{-1} (U_{eff}). Since the tunnelling probability is high, one can expect a reduction in the U_{eff} value compare to the U_{cal} value, where this probability is not taken in to consideration.

For complex **7** {Al$_2$Dy$_2$}, the tunnelling probability of the exchange coupled ground state is almost negligible ($\Delta_{tun} = 3.6 \times 10^{-6}$). This places the estimate of U_{cal} for this molecule as 43.5 cm^{-1} and relaxation *via* the exchange coupled first excited state ($\Delta_{tun} = 6.3 \times 10^{-5}$, see Fig. 10d). This picture is consistent with the experimental data where in absence of an external field relaxation occurs with a barrier height of 26.9 cm^{-1}.

It is important to note here that there are some deviations in the experimental and theoretically estimated barrier heights. This is essentially due to the fact that our relaxation mechanism has not factored other possibilities such as intermolecular interaction, hyperfine coupling of the metal ions/nitrogen atoms *etc.*, that are likely to contribute the overall relaxation process and thus this difference between U_{eff} and U_{cal} is inevitable.

Conclusions

Five new butterfly complexes: [M$_2^{III}$Ln$_2^{III}$(μ_3-OH)$_2$(p-Me-PhCO$_2$)$_6$(-L)$_2$] (H$_2$L = 2,2'-((pyridin-2-ylmethyl)azanediyl)bis(ethan-1-ol), M = Cr, Ln = Dy (**1**) or Y (**2**), M = Mn, Ln = Dy (**3**) or Y (**4**)) and the diluted complex [Al$_2^{III}$Dy$_2^{III}$]:[Al$_2^{III}$Dy$_{0.18}^{III}$Y$_{1.82}$(μ_3-OH)$_2$(p-Me-PhCO$_2$)$_6$(L)$_2$] **8** have been synthesised, characterised and their magnetic slow relaxation properties investigated. This has allowed us to set these compounds into the context of the properties of our previously reported {Fe$_2^{III}$Ln$_2^{III}$}, Ln = Dy **5** or Y **6** and {Al$_2^{III}$Dy$_2^{III}$} **7** analogues. The nature of the 3d metal ion sitting at the body positions of the butterfly motif steers the slow magnetic relaxation properties of the whole molecule by "tempering" the relaxation of the wingtip Dy ions. This is the first systematic study on changing the nature of the 3d^{III} body ions from Cr(d^3), Mn(d^4), Fe(d^5) and diamagnetic Al^{III} within this motif.

Ac susceptibility measurements indicate no SMM behaviour was observed for any of the analogues using diamagnetic yttrium at the wingtips instead of Dy. This reveals that the SMM behaviour is intrinsic to the presence of the Dy^{III} ions. Furthermore, for the {Al$_2$Dy$_2$} analogue, the weak (+0.049 cm^{-1}) dipolar interaction between the two far away Dy^{III} ions plays a key role in suppressing the zero-field QTM of the individual Dy^{III} ions as revealed by this compound showing SMM behaviour under zero

dc field. Thus the weak but key cooperative interaction plays a significant role for the performance of the system in terms of the dynamic and thus SMM behaviour. Changing from Cr to Mn in the {M$_2^{III}$Ln$_2^{III}$} motif, the anisotropy of the Dy^{III} ion can be utilised to improve the performance of the SMM through tuning the suppression (quenching) of the QTM processes of the Dy^{III} ions. The SMM behaviour for the four complexes follows the trend, {Al$_2$Dy$_2$} > {Mn$_2$Dy$_2$} > {Fe$_2$Dy$_2$} > {Cr$_2$Dy$_2$}. *Ab initio* calculations performed on all Dy^{III}-containing molecules reveal similar results. It is clear that the strength and maybe the sign of the 3d–4f exchange interaction plays a key role in directing the nature of the SMM properties observed.

Experimental

General information

All chemicals and solvents used for synthesis were obtained from commercial sources and used as received without further purification. All reactions were carried out under aerobic conditions. *N*-(2-Pyridylmethyl)iminodiethanol was prepared according to the literature procedure.[43] The elemental analyses (C, H, and N) were carried out using an Elementar Vario EL analyser. Fourier transform IR spectra (4000 to 400 cm^{-1}) were measured on a PerkinElmer Spectrum GX spectrometer with samples prepared as KBr discs. Powder X-ray diffraction was carried out on a STOE STADI-P diffractometer, using Cu-Kα radiation with $\lambda = 1.5406$ Å.

[Cr$_2^{III}$Dy$_2$(μ_3-OH)$_2$(L)$_2$(p-Me-PhCO$_2$)$_6$]·2MeCN (1)

H$_2$L (100 mg, 0.5 mmol) in MeCN (5 ml) was added to a solution of CrCl$_3$·6H$_2$O (66 mg, 0.25 mmol), DyCl$_3$·6H$_2$O (94 mg, 0.25 mmol) and 4-methylbenzoic acid (136 mg, 1 mmol) in a mixture of MeCN (20 ml) and MeOH (5 ml). After 10 min of stirring, Et$_3$N (0.42 ml, 3 mmol) was added, leaving the solution stirring for a further 1 min. The final solution was filtered and left undisturbed. After three days, pale green crystals suitable for X-ray analysis were collected and air dried. Yield: 50% (145.4 mg, based on 4-methylbenzoic acid). Anal. calcd for Cr$_2$Dy$_2$C$_{68}$H$_{72}$-N$_4$O$_{18}$·2MeCN: C, 49.57; H, 4.51; N, 4.82. Found: C, 49.44; H, 4.37; N, 5.02. Selected IR data (KBr, cm^{-1}) for **1**: 3493 (br), 3062 (w), 2978 (w), 2856 (m), 1595 (s), 1542 (s), 1097 (s), 908 (s), 719 (s), 673 (s), 593 (s).

[Cr$_2^{III}$Y$_2$(μ_3-OH)$_2$(L)$_2$(p-Me-PhCO$_2$)$_6$]·2MeCN (2)

The same reaction conditions as used for compound **1**, substituting DyCl$_3$·6H$_2$O with YCl$_3$·6H$_2$O produced compound **2**. Yield: 55% (based on 4-methylbenzoic acid). Cr$_2$Y$_2$C$_{68}$H$_{72}$-N$_4$O$_{18}$·2MeCN: C, 54.14; H, 4.92; N, 5.26. Found: C, 54.24; H, 4.87; N, 5.00. The IR spectrum is similar to that of compound **1**.

[Mn$_2^{III}$Dy$_2$(μ_3-OH)$_2$(L)$_2$(p-Me-PhCO$_2$)$_6$]·2MeCN·2MeOH (3)

The same reaction conditions used for compound **1** replacing CrCl$_3$·6H$_2$O with MnCl$_2$·4H$_2$O and halving the amount of Et$_3$N produced compound **3**. Yield: 61% (187.5 mg, based on 4-methylbenzoic acid). Anal. calcd for Mn$_2$Dy$_2$C$_{68}$H$_{72}$N$_4$O$_{18}$-·2MeCN (lose two MeOH): C, 49.41; H, 4.49; N, 4.80. Found: C,

49.29; H, 4.51; N, 4.59. Selected IR data (KBr, cm^{-1}) for **3**: 3503 (br), 3058 (w), 2975 (w), 2854 (m), 1593 (s), 1541 (s), 1099 (s), 906 (s), 722 (s), 672 (s), 593 (s).

$[Mn_2^{III}Y_2(\mu_3\text{-}O)_2(L)_2(p\text{-}Me\text{-}PhCO_2)_6]\cdot 2MeCN\cdot 2MeOH$ (4)

The same reaction conditions as used for compound **3** replacing DyCl$_3$·6H$_2$O with YCl$_3$·6H$_2$O produced compound **4**. Mn$_2$Y$_2$-C$_{68}$H$_{72}$N$_4$O$_{18}$·2MeCN (with the loss of two MeOH): C, 53.94; H, 4.90; N, 5.24. Found: C, 53.79; H, 4.91; N, 5.30. The IR spectrum is similar to that of compound **4**.

$[Al_2^{III}Dy_{0.18}Y_{1.82}(\mu_3\text{-}OH)_2(L)_2(p\text{-}Me\text{-}PhCO_2)_6]\cdot 2MeCN$ (8)

H$_2$L (100 mg, 0.5 mmol) in MeCN (5 ml) was added to a solution of AlCl$_3$·6H$_2$O (66 mg, 0.25 mmol), DyCl$_3$·6H$_2$O (9.4 mg, 0.025 mmol), YCl$_3$·6H$_2$O (68.3 mg, 0.225 mmol) and 4-methylbenzoic acid (136 mg, 1 mmol) in a mixture of MeCN (20 ml) and MeOH (5 ml). After 10 min of stirring, NEt$_3$ (0.42 ml, 3 mmol) was added and the solution stirred for a further 1 min. The final solution was filtered and left undisturbed. After three days, white crystals suitable for X-ray analysis were collected and air dried. Yield: 45.1% (101.2 mg, based on 4-methylbenzoic acid). Al$_2$Dy$_{0.18}$Y$_{1.82}$C$_{68}$H$_{72}$N$_4$O$_{18}$·2MeCN: C, 55.42; H, 5.04; N, 5.39. Found: C, 55.59; H, 4.97; N, 5.20. The IR is similar to that of the reported **7** {Al$_2$Dy$_2$}.

Magnetic measurements

The magnetic susceptibility measurements were obtained using a Quantum Design SQUID magnetometer MPMS-XL in the temperature range 1.8–300 K. Measurements were performed on polycrystalline samples restrained in eicosane and placed in sealed plastic bags. Magnetisation isotherms were collected at 2, 5 K between 0 and 7 T. Alternating current (ac) susceptibility measurements were performed with an oscillating field of 3 Oe and ac frequencies ranging from 0.05 to 1500 Hz. The magnetic data were corrected for the sample holder and the diamagnetic contribution.

X-ray analysis

The X-ray data were collected on an Oxford Diffraction Supernova E diffractometer, using Mo-K$_\alpha$ radiation ($\lambda = 0.71073$ Å) from a microfocus source. Structures were solved by dual-space direct methods using SHELXT[44] and refined against F_o^2 using SHELXL-2014[45] with anisotropic displacement parameters for all non-hydrogen atoms. Organic hydrogen atoms were placed in calculated positions; the coordinates of H(1) were refined. Crystallographic data (excluding structure factors) for the structures in this paper have been deposited with the Cambridge Crystallographic Data Centre as supplementary publication nos.†

Computational details

We performed *ab initio* CASSCF[31] + RASSI-SO[32] + SINGLE_-ANISO[33–36] calculations on all paramagnetic ions using the single crystal structure data in MOLCAS 8.0[46–50] suite by substituting all the paramagnetic ions with diamagnetic ions

(La^{III}/Sc^{III}) except for the one of interest as attempted earlier by keeping other parts unchanged. We used the [C.ANO-RCC…3s2p], [N.ANO-RCC…3s2p1d], [O.ANO-RCC…3s2p1d], [H.ANO-RCC…2s], [Al.ANO-RCC…4s3p1d], [Sc.ANO-RCC…5s4p2d1f], [Fe.ANO-RCC…5s4p2d1f], [Cr.ANO-RCC…5s4p2d1f], [Mn.ANO-RCC…5s4p2d1f], [Lu.ANO-RCC…7s6p4d2f1g] and [Dy.ANO-RCC…8s7p5d3f2g1h] basis set for our *ab initio* calculations.[51] For our CASSCF calculations on Dy-mononuclear fragment, nine electrons in seven active 4f orbitals were considered. Further, here in the RASSI-SO step, 21 roots for sextet spin multiplicity were considered.[52] For the Cr-mononuclear fragment, the active space of the CASSCF method was constructed considering three electrons in five active 3d orbitals with 10 and 40 roots for quadruplet and doublet spin multiplicities respectively. For the Mn-mononuclear fragment, the active space of the CASSCF method was constructed considering four electrons in five active 3d orbitals. Further, here in the RASSI-SO step, we considered only 5 and 35 roots for pentet and triplet spin multiplicities respectively. For the Fe-mononuclear fragment, five electrons in five active 3d orbitals are considered. For the next RASSI-SO step we only considered 1 and 17 roots for sextet and quadruplet spin multiplicities respectively.[33–36] The resultant spin–orbit multiplet has been further used to compute local magnetic properties *via* SINGLE_ANISO approach. The magnetic exchange interactions (J_s) have been computed between all paramagnetic ions for all complexes by fitting *ab initio* POLY_ANISO with the experimental data.[37]

Conflicts of interest

There are no conflicts to declare.

Acknowledgements

Notes and references

1 C. Benelli and D. Gatteschi, *Chem. Rev.*, 2002, **102**, 2369–2387.
2 R. Sessoli and A. K. Powell, *Coord. Chem. Rev.*, 2009, **253**, 2328–2341.
3 J. S. Miller and D. Gatteschi, *Chem. Soc. Rev.*, 2011, **40**, 3076–3091.
4 L. Rosado Piquer and E. C. Sañudo, *Dalton Trans.*, 2015, **44**, 8771–8780.
5 D. E. Freedman, W. H. Harman, T. D. Harris, G. J. Long, C. J. Chang and J. R. Long, *J. Am. Chem. Soc.*, 2010, **132**, 1224–1225.
6 N. Ishikawa, *Polyhedron*, 2007, **26**, 2147–2153.

7 J. L. Liu, Y. C. Chen, Y. Z. Zheng, W. Q. Lin, L. Ungur, W. Wernsdorfer, L. F. Chibotaru and M. L. Tong, *Chem. Sci.*, 2013, **4**, 3310–3316.

8 N. E. Chakov, M. Soler, W. Wernsdorfer, K. A. Abboud and G. Christou, *Inorg. Chem.*, 2005, **44**, 5304–5321.

9 P. King, W. Wernsdorfer, K. A. Abboud and G. Christou, *Inorg. Chem.*, 2005, **44**, 8659–8669.

10 F. Pointillart, K. Bernot, R. Sessoli and D. Gatteschi, *Chem.–Eur. J.*, 2007, **13**, 1602–1609.

11 J. L. Liu, J. Y. Wu, Y. C. Chen, V. Mereacre, A. K. Powell, L. Ungur, L. F. Chibotaru, X. M. Chen and M. L. Tong, *Angew. Chem., Int. Ed.*, 2014, **53**, 12966–12970.

12 S. K. Langley, D. P. Wielechowski, N. F. Chilton, B. Moubaraki and K. S. Murray, *Inorg. Chem.*, 2015, **54**, 10497–10503.

13 B. Moubaraki, S. K. Langley, C. Le, B. F. Abrahams, L. F. Chibotaru, L. Ungur and K. S. Murray, *Inorg. Chem.*, 2015, **54**, 3631–3642.

14 S. K. Langley, D. P. Wielechowski, B. Moubaraki and K. S. Murray, *Chem. Commun.*, 2016, **52**, 10976–10979.

15 E. Moreno-Pineda, N. F. Chilton, F. Tuna, R. E. P. Winpenny and E. J. L. McInnes, *Inorg. Chem.*, 2015, **54**, 5930–5941.

16 A. Baniodeh, Y. Lan, G. Novitchi, V. Mereacre, A. Sukhanov, M. Ferbinteanu, V. Voronkova, C. E. Anson and A. K. Powell, *Dalton Trans.*, 2013, **42**, 8926–8938.

17 Y. Peng, V. Mereacre, C. E. Anson and A. K. Powell, *Phys. Chem. Chem. Phys.*, 2016, **18**, 21469–21480.

18 D. Casanova, P. Alemany, J. M. Bofill and S. Alvarez, *Chem.–Eur. J.*, 2003, **9**, 1281–1295.

19 S. Alvarez, D. Avnir, M. Llunell and M. Pinsky, *New J. Chem.*, 2002, **26**, 996–1009.

20 S. Alvarez, P. Alemany, D. Casanova, J. Cirera, M. Llunell and D. Avnir, *Coord. Chem. Rev.*, 2005, **249**, 1693–1708.

21 N. F. Chilton, R. P. Anderson, L. D. Turner, A. Soncini and K. S. Murray, *J. Comput. Chem.*, 2013, **34**, 1164–1175.

22 M. L. Kahn, J. P. Sutter, S. Golhen, P. Guionneau, L. Ouahab, O. Kahn and D. Chasseau, *J. Am. Chem. Soc.*, 2000, **122**, 3413–3421.

23 M. L. Kahn, R. Ballou, P. Porcher, O. Kahn and J. Sutter, *Chem.–Eur. J.*, 2002, **8**, 525–531.

24 http://www.nfchilton.com/phi.html.

25 D. Gattenschi, R. Sessoli and J. Villain, *Molecular Nanomagnets*, Oxford, New York, 2006.

26 A. Mishra, W. Wernsdorfer, S. Parsons, G. Christou and E. K. Brechin, *Chem. Commun.*, 2005, 2086–2088.

27 A. Yamashita, A. Watanabe, S. Akine, T. Nabeshima, M. Nakano, T. Yamamura and T. Kajiwara, *Angew. Chem., Int. Ed.*, 2011, **50**, 4016–4019.

28 H. L. C. Feltham, R. Clérac, L. Ungur, L. F. Chibotaru, A. K. Powell and S. Brooker, *Inorg. Chem.*, 2013, **52**, 3236–3240.

29 H. L. C. Feltham, F. Klöwer, S. A. Cameron, D. S. Larsen, Y. Lan, M. Tropiano, S. Faulkner, A. K. Powell and S. Brooker, *Dalton Trans.*, 2011, **40**, 11425–11432.

30 E. Moreno-Pineda, N. F. Chilton, R. Marx, M. Dörfel, D. O. Sells, P. Neugebauer, S. D. Jiang, D. Collison, J. Van Slageren, E. J. L. McInnes and R. E. P. Winpenny, *Nat. Commun.*, 2014, **5**, 1–7.

31 B. Swerts, L. F. Chibotaru, R. Lindh, L. Seijo, Z. Barandiaran, S. Clima, K. Pierloot and M. F. A. Hendrickx, *J. Chem. Theory Comput.*, 2008, **4**, 586–594.

32 P. Å. Malmqvist, B. O. Roos and B. Schimmelpfennig, *Chem. Phys. Lett.*, 2002, **357**, 230–240.

33 L. F. Chibotaru, A. Ceulemans and H. Bolvin, *Phys. Rev. Lett.*, 2008, **101**, 4–7.

34 L. F. Chibotaru and L. Ungur, *J. Chem. Phys.*, 2012, **137**, 064112–064122.

35 L. F. Chibotaru and L. Ungur, *Program SINGLE_ANISO*, KU Leuven, Leuven, Belgium, 2006.

36 L. Ungur and L. F. Chibotaru, http://www.molcas.org/documentation/manual/node105.html.

37 L. F. Chibotaru and L. Ungur, *Program POLY_ANISO*, KU Leuven, Leuven, Belgium, 2007.

38 L. Gagliardi, R. Lindh and G. Karlström, *J. Chem. Phys.*, 2004, **121**, 4494–4500.

39 K. R. Vignesh, S. K. Langley, K. S. Murray and G. Rajaraman, *Inorg. Chem.*, 2017, **56**, 2518–2532.

40 T. Gupta and G. Rajaraman, *Chem. Commun.*, 2016, **52**, 8972–9008.

41 X.-Q. Zhao, S. Xiang, J. Wang, D.-X. Bao and Y.-C. Li, *ChemistryOpen*, 2018, **7**, 192–200.

42 A. Chakraborty, J. Goura, P. Kalita, A. Swain, G. Rajaraman and V. Chandrasekhar, *Dalton Trans.*, 2018, **47**, 8841–8864.

43 K. Sundaravel, M. Sankaralingam, E. Suresh and M. Palaniandavar, *Dalton Trans.*, 2011, **40**, 8444–8458.

44 G. M. Sheldrick, *Acta Crystallogr., Sect. A: Found. Adv.*, 2015, **71**, 3–8.

45 G. M. Sheldrick, *Acta Crystallogr., Sect. C: Struct. Chem.*, 2015, **71**, 3–8.

46 F. Aquilante, J. Autschbach, R. K. Carlson, L. F. Chibotaru, M. G. Delcey, L. De Vico, I. F. Galván, N. Ferré, L. M. Frutos, L. Gagliardi, M. Garavelli, A. Giussani, C. E. Hoyer, G. Li Manni, H. Lischka, D. Ma, P. Å. Malmqvist, T. Müller, A. Nenov, M. Olivucci, T. B. Pedersen, D. Peng, F. Plasser, B. Pritchard, M. Reiher, I. Rivalta, I. Schapiro, J. Segarra-Martí, M. Stenrup, D. G. Truhlar, L. Ungur, A. Valentini, S. Vancoillie, V. Veryazov, V. P. Vysotskiy, O. Weingart, F. Zapata and R. Lindh, *J. Comput. Chem.*, 2016, **37**, 506–541.

47 J. A. Duncan, *J. Am. Chem. Soc.*, 2009, **131**, 2416.

48 V. Veryazov, P. O. Widmark, L. Serrano-Andrés, R. Lindh and B. O. Roos, *Int. J. Quantum Chem.*, 2004, **100**, 626–635.

49 G. Karlström, R. Lindh, P. Å. Malmqvist, B. O. Roos, U. Ryde, V. Veryazov, P. O. Widmark, M. Cossi, B. Schimmelpfennig, P. Neogrady and L. Seijo, *Comput. Mater. Sci.*, 2003, **28**, 222–239.

50 F. Aquilante, L. De Vico, N. Ferré, G. Ghigo, M. Reiher, B. O. Roos, L. Serrano-Andrés, M. Urban, V. Veryazov and R. Lindh, *J. Comput. Chem.*, 2010, **31**, 224–227.

51 B. O. Roos, R. Lindh, P. Å. Malmqvist, V. Veryazov, P. O. Widmark and A. C. Borin, *J. Phys. Chem. A*, 2008, **112**, 11431–11435.

52 K. Bernot, J. Luzon, L. Bogani, M. Etienne, C. Sangregorio, M. Shanmugam, A. Caneschi, R. Sessoli and D. Gatteschi, *J. Am. Chem. Soc.*, 2009, **131**, 5573–5579.